

# Deformation and Fracture of Nano-sculptured Thin Film

T. Kitamura<sup>1</sup>, T. Sumigawa<sup>1</sup>  
<sup>1</sup>*Kyoto University, Kyoto, Japan*

**Abstract** The mechanical property of a sculptured thin film has been investigated in this project, and the focus is put on the deformation and fracture. Using an experimental method we proposed, the deformation property of a thin film consisting of Ta<sub>2</sub>O<sub>5</sub> nano-springs is evaluated. The thin film show strong deformation anisotropy that solid ones could hardly attain. The fact that the thin film eliminates stress singularity at the interface edge between dissimilar materials is analytically elucidated, and interface crack initiation and propagation experiments are carried out. Both of them are governed by an apparent allowable strain of the nanosprings at the edges.

## 1. Introduction

New deposition techniques enable us to fabricate nano-sized structures. In particular, a thin film consisting of nano-elements is formed on a substrate by means of the dynamic oblique deposition (DOD) [1-2]. It has the potential to play a key role in mechanical electronic devices because the thin films would exhibit significantly characteristic mechanical properties in comparison with solid films. The geometrical anisotropy of constituent nano-elements would cause the mechanical anisotropy of film, and insertion of the thin film between dissimilar materials as an interface layer may break down a continuum approximation of the stress field near the interface owing to discrete structure of the film. However, the investigation of the mechanical properties of nano-elements has not been enough yet.

In this paper, we review our experimental and theoretical works on the mechanical properties of nano-elements.

## 2. Mechanical property of thin film consisting of nanosprings [3-4]

### 2.1 Experimental procedure

As a base layer, a Ta<sub>2</sub>O<sub>5</sub> solid film is deposited on a silicon (100) substrate by electron beam (EB) evaporation. Then, nanosprings (helical nano-elements) of Ta<sub>2</sub>O<sub>5</sub> are grown by the dynamic oblique deposition (DOD). A Ta<sub>2</sub>O<sub>5</sub> cap layer with a thickness of 280 nm is deposited on the nanosprings. Figure 1(a) shows a scanning electron micrograph of the multi-layered thin films. The height of the nanosprings,  $h_s$ , is 560 nm. The areal number density of springs is 65 per  $\mu\text{m}^2$ . The number of turns, the outside radius, and diameter of wire of the nanospring are 3.5, 75 nm, and  $60\pm 10$  nm, respectively.

Figure 1(b) shows the specimen configuration. Specimens for the loading tests are cut from the multi-layered thin films by a focused ion beam (FIB). Several specimens with different areas ( $S = 1.9\text{-}13.2 \mu\text{m}^2$ ) are prepared.

The tests are conducted using an atomic force microscope with a loading apparatus (Hysitron: Triboscope). Figures 1(c) and 1(d) schematize the loading test. The vertical and lateral forces,  $F_v$  and  $F_l$ , are applied to the cap layer by the

diamond tip. In the vertical loading tests, the vertical force is applied to the cap layer at a constant loading velocity of 10  $\mu\text{N/s}$  (see Fig. 1(c)). In the lateral loading tests, the lateral force is applied to the side edge of the cap layer (see Fig. 1(d)). The loading tip is moved along the substrate surface toward the specimen at a constant velocity of 5 nm/s.

## 2.2 Results

Figure 2(a) plots the  $F_v$  against the vertical displacement,  $\delta_v$ , for a specimen with  $S = 3.3 \mu\text{m}^2$ . The fact that the relation between  $F_v$  and  $\delta_v$  is almost linear indicates that the specimen deforms elastically. The vertical stiffness of the thin film,  $K_v$  ( $=F_v/\delta_v$ ), is evaluated by the least-squares approximation. The relationship between  $K_v$  and  $S$  is shown by solid circles in Fig. 2(c).  $K_v$  has an almost linear relationship with  $S$ . The apparent Young's modulus,  $E'$ , and stiffness constant,  $k_v$ , of a spring are defined as  $E' = K_v(h_s/S)$  and  $k_v = K_v/m$ , respectively. The mean values of  $E'$  and  $k_v$  obtained from the vertical loading tests are 0.375 GPa and 10.29 N/m, respectively.

Figure 2(b) shows the  $F_l$  plotted against the lateral displacement,  $\delta_l$ , in the lateral loading test of a specimen with  $S = 6.4 \mu\text{m}^2$ .  $F_l$  increases almost linearly with  $\delta_l$ . The lateral stiffness of the thin film,  $K_l$  ( $=F_l/\delta_l$ ), is evaluated. The open squares in Fig. 2(c) show the relationship between  $K_l$  and  $S$ .  $K_l$  increases almost linearly with increasing  $S$ . The apparent shear modulus of the thin film,  $G'$ , and the lateral stiffness measurement,  $k_l$ , of a spring are defined as  $G' = K_l(h_s/S)$  and  $k_l = K_l/m$ , respectively. The mean values of  $G'$  and  $k_l$  obtained from the lateral loading tests are 0.060 GPa and 1.66 N/m, respectively.

The  $E'$  and  $G'$  of the thin film consisting of  $\text{Ta}_2\text{O}_5$  nanosprings are 2-3 orders of magnitude lower than those of the solid  $\text{Ta}_2\text{O}_5$  film ( $E = 117$  GPa and  $G = 47$  GPa). The ratio of  $E'$  to  $G'$  is 6.2, while that of isotropic solid materials given as  $2(1+\nu)$  must be at most 3.0 because the maximum value of  $\nu$  is 0.5. This means that the thin film composed of  $\text{Ta}_2\text{O}_5$  helical nanosprings has a strong anisotropy.

## 3. Effect of thin film consisting of nanosprings on stress fields at interface edge and crack tip [4]

### 3.1 Analytical procedure

Stress analysis is conducted under plane strain condition through FEM using ABAQUS 6.5. Each nanospring is replaced by the equivalent cylindrical beam with a height of  $h_b=560$  nm, a diameter of  $D_b = 259$  nm, and a Young's modulus of  $E_b$  0.11 GPa. The  $D_b$  and  $E_b$  can be derived from the vertical and lateral stiffness measurements of a single spring,  $k_v$  and  $k_l$ .

Figure 3 shows the model used for analyzing the stress distribution near the interface edges between the thin film and a solid body. The thin film consisting of  $\text{Ta}_2\text{O}_5$  nanosprings with a thickness of 560 nm is sandwiched between an elastic solid body and a substrate. Figure 3(c) shows the mesh division for the models. Two types of models with different interface edges between the thin film and the solid body are prepared. One has a free edge where the surface-interface angle is  $90^\circ$ - $90^\circ$  (see Fig. 3(a)), and the other has an interface crack with a length of 4  $\mu\text{m}$  (see Fig. 3(b)). The Young's modulus and Poisson's ratio of the  $\text{Ta}_2\text{O}_5$  solid body

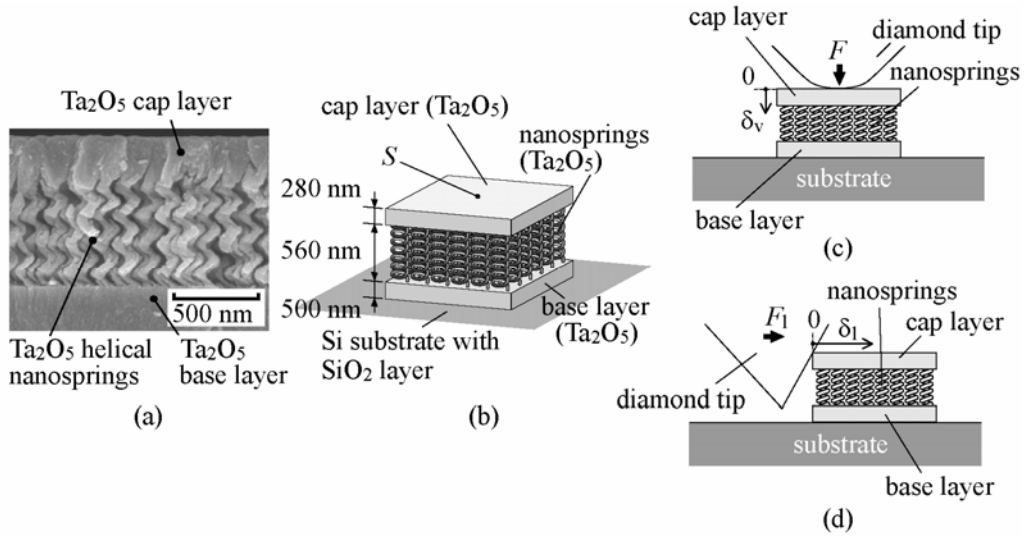


Fig.1 (a) SEM micrograph of multi-layered thin films. (b) Configuration of specimen. (c) Vertical loading method. (d) Lateral loading method.

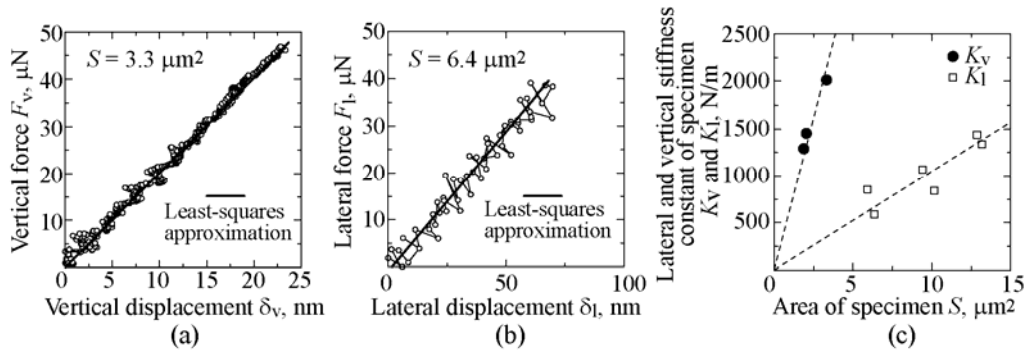


Fig.2 Relationship between force and displacement: (a) Vertical loading method, (b) Lateral loading method. (c) Relationship between stiffness and area of specimen.

are 117 GPa and 0.23, respectively. The distance between springs is 125 nm, which is derived from the areal number density of springs. In addition, models without nanosprings are prepared for comparison (Figs. 3(d), (e), and (f)). The models with and without the thin film consisting of nanosprings are designed as "spring model" and "non-spring model", respectively. The uniform displacement  $\Delta u_z$  is applied to the top of the model.

### 3.2 Results

The stresses in the elements of the elastic solid body along the interface are extracted. Figures 4(a) and (b) show the distributions of the normal stresses,  $\sigma_x$  and  $\sigma_z$ , and the shear stress,  $\tau_{xz}$ , along the interface in the models with a free edge. The stresses are normalized by the  $z$ -directional normal stress at the center of the interface,  $\sigma_0$ , in each model. In the no-spring model (Fig. 4(a)), the stresses increase near the free edge. A stress singularity represented by  $\sigma_{ij}/\sigma_0 = K/r$  ( $i, j = z, x$ ) [5] is observed near the free edge in each distribution curve. Here,  $K$  is the stress intensity factor,  $r$  is the distance from the free edge, and  $\lambda$  is a parameter

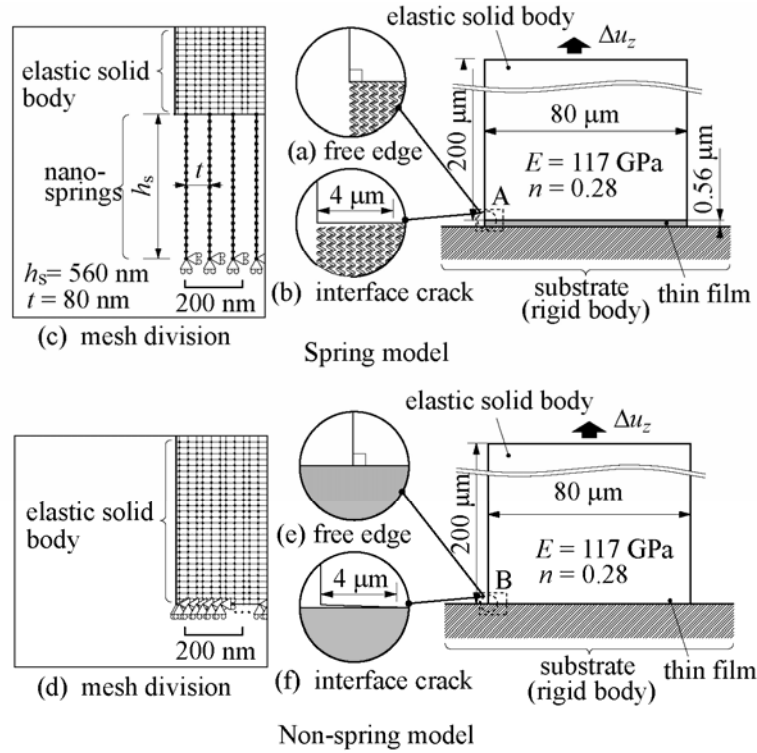


Fig. 3 Analytical models for FEM.

that depends on the materials and the edge geometry. In the spring model (Fig. 4(b)), there is no stress singularity near the free edge.

Figures 4(c) and (d) show the distributions of the normalized stresses along the interface in the models containing an interface crack. In the non-spring model (Fig. 4(c)), the stresses are concentrated in the region near the crack tip. Stress singularity is observed near the crack tip. In the spring model (Fig. 4(d)),  $\sigma_z$  and  $\tau_{zx}$  are almost constant over the interface as in the case of the model with the free edge. No singular stress field occurs in any of the distributions.

The stress concentration at the free edge of an interface is induced by the mismatch of deformation on the interface. The mismatch is mainly due to the difference in Poisson's contractions between the different components. Since nano-springs are oriented vertically on the substrate and are separated from each other, the in-plane deformation of the thin film follows that of the adjoining component on the interface. In short, the difference of Poisson's contractions for the vertical deformation is zero. The stress concentration at the interface crack tip is induced by not only the mismatch of deformation on the interface but also the traction force from above and below the crack. However, no traction force is exerted on the crack tip in the spring model because the under part of the crack is constitutively separated from the crack tip.

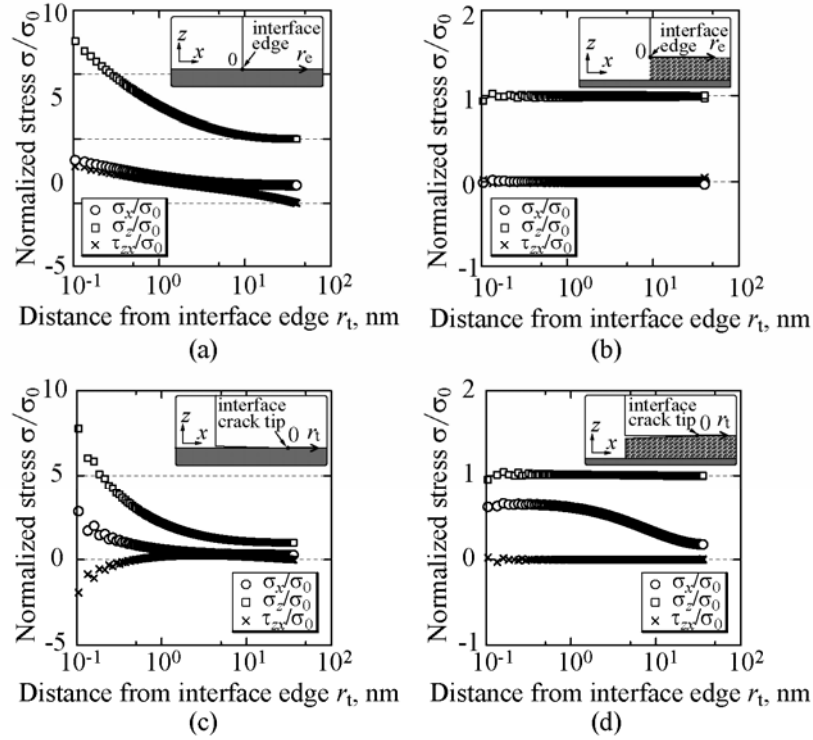


Fig. 4 Distribution of normal stresses,  $z$  and  $x$ , and shear stress,  $zx$ , along the interface: (a) near the interface edge in non-spring model, (b) near the interface edge in spring model, (c) near the interface crack tip in non-spring model, (b) near the interface crack tip in spring model.

#### 4. Effect of thin film consisting of nanosprings on crack initiation at interface edge [6]

##### 4.1 Experimental procedure

A thin film consisting of  $Ta_2O_5$  nanosprings is formed on a Si substrate by means of the DOD. A  $Ta_2O_5$  solid film with a height of 1700 nm is then deposited on the thin film by the EB evaporation (see Fig. 5(a)). The number of turns, the outside radius, and diameter of wire of the nanospring are 3.5, 90 nm, and  $40 \pm 10$  nm, respectively.

Table 1 Dimensions of specimens used for the crack initiation experiment. Dimensions are in mm.

Specimen	$L$	$b$	$t$	$l$
A-1	2.27	1.58	1.92	17.5
A-2	2.17	2.09	1.87	11.0
A-3	1.37	1.77	1.90	15.5
B-1	1.74	1.68	1.90	15.5
B-2	1.85	1.95	1.89	16.0

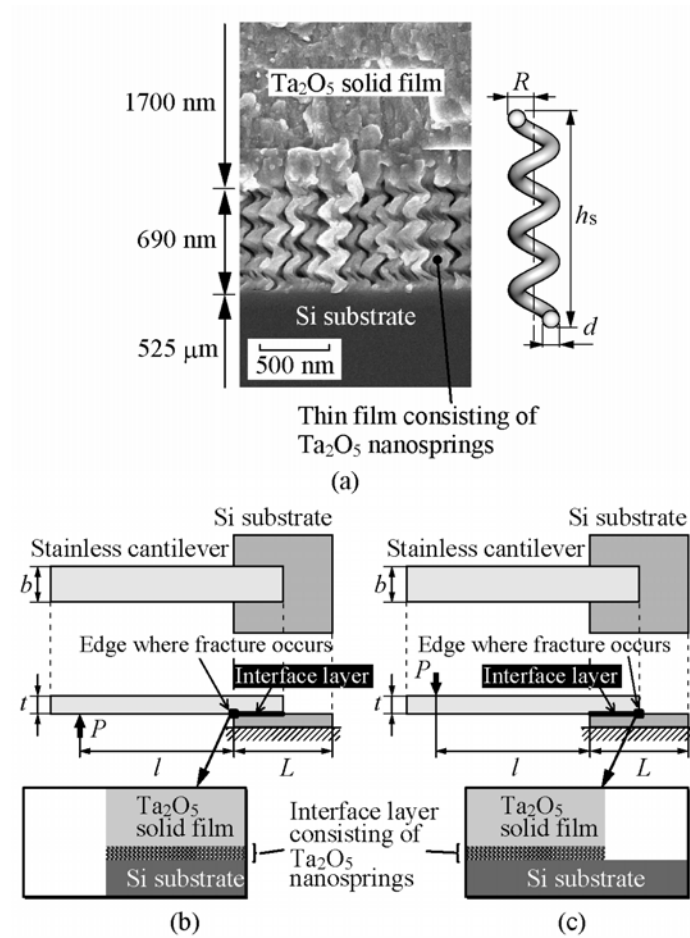


Fig.5 (a) SEM micrograph of dissimilar material including a thin film comprising of  $\text{Ta}_2\text{O}_5$  nanosprings. (b), (c) Illustrations of specimen and loading method.

The material is cut to a square coupon with a size of  $5\text{ mm} \times 5\text{ mm}$ . A stainless cantilever is bonded to the thin film of the coupon using an epoxy adhesive. The thin film except the bonded region is mechanically removed.

Figures 5(b) and (c) illustrates the specimen configuration and the loading method. We carry out two types of experiments, which are designated as "Type A test" and "Type B test", respectively. Table 1 lists the sizes of the specimens. A vertical load applied to the lower face of the stainless steel cantilever (Fig.5(b)) initiates a crack at the left edge of the thin film. On the other hand, a vertical load applied to the upper face of the cantilever (Fig.5(c)) initiates a crack at the right edge of the thin film.

The experiments are conducted at a room temperature in an air by means of a loading machine with an electromagnetic actuator. The vertical load is applied to the stainless cantilever at the point of  $l$  from the edge of the thin film with a constant displacement rate of  $50\ \mu\text{m/s}$ .

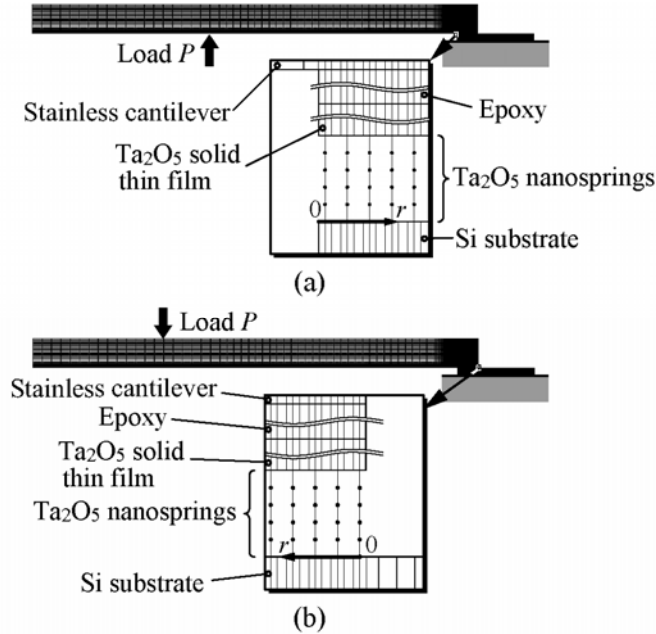


Fig. 6 Mesh division for FEM analysis: Type A test, and (b) Type B test.

#### 4.2 Analytical procedure

Figure 6 illustrates mesh divisions for analytical models. The nanosprings are translated to equivalent beam elements. The Young's modulus and Poisson's ratio of the  $\text{Ta}_2\text{O}_5$  solid body are 117 GPa and 0.23, respectively. In addition, models where the  $\text{Ta}_2\text{O}_5$  solid film is directly laminated on the Si substrate without the thin film are analyzed for comparison. Hereafter, the analytical models with and without the thin film are designated as "thin film model" and "non-thin film model", respectively.

#### 4.3 Results

In the experiments, the displacement at the loading point,  $u_y$ , increases linearly with increasing the applied load,  $P$ . The sharpen drop of the load at the maximum value points out that the interface crack is initiated.

Figure 7(a) shows the typical relationship between the normal stress,  $\sigma_y$ , and the distance from the interface edge,  $x$ , at the crack initiation in the non-thin film model.  $\sigma_y$  is extracted from the elements adjoining the interface in the Si substrate. No stress singularity takes place at the left edge of the interface with the  $90^\circ$ - $90^\circ$  interface edge shape of the  $\text{Ta}_2\text{O}_5$  solid film and the Si substrate (Type A). On the other hand, the right edge of the interface where the interface edge shape is  $90^\circ$ - $180^\circ$  generates a stress singularity due to the edge shape (Type B).

Figure 7(b) shows the typical relationship between the apparent normal stress of the nanospring,  $\sigma'$ , and the distance from the interface edge,  $x$ , at the crack initiation in the thin film model. Using the longitudinal displacement of the nanospring,  $\lambda$ , the height,  $h_s$ , the Young's modulus,  $E_b$ , the diameter,  $D_b$  of the beam element, and the outer diameter of the nanospring,  $d$ , the apparent normal stress,  $\sigma'$ , in the longitudinal direction of the nanospring is represented as follow:

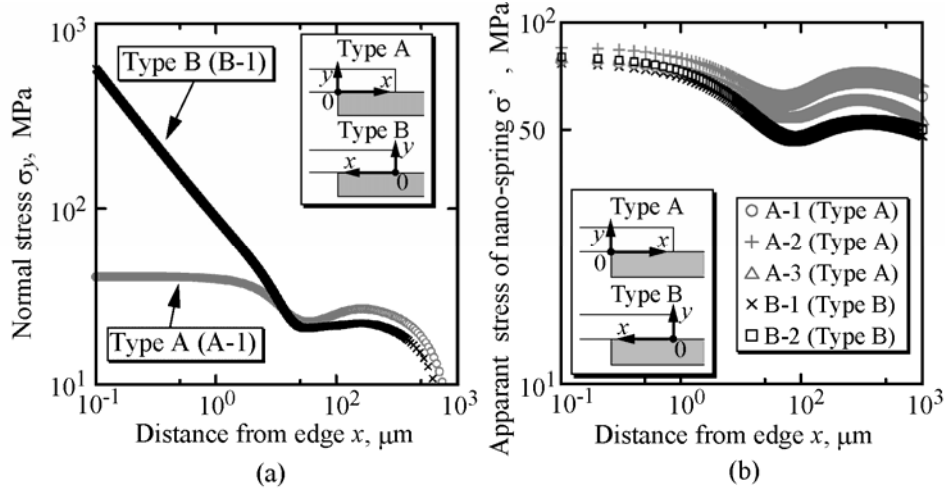


Fig. 7 Relationship between normal stress,  $\sigma$ , and distance from the edge of thin film,  $r$ : (a) non-thin film model, and (b) thin film model.

$$\sigma' = (E_b \lambda / h_s) (D_b^2 / d^2). \quad (1)$$

In Fig. 7(b), the stresses near the edge are nearly constant. The no strong stress concentration points out that the thin film consisting of nanosprings eliminates the stress singularity. Moreover, the stress distribution curves of all specimens show a good agreement near the interface edge. This signifies that the stress near the edge dominates the crack initiation. The magnitude of critical stress is evaluated as  $78.5 \pm 4.0$  MPa ( $\epsilon_c' = 5.1 \pm 0.2 \times 10^{-2}$ ).

## 5. Summary

The mechanical properties of nano-elements have been investigated in this project. Novel experiments and stress analyses for the nano-elements elucidate the specific behavior of deformation and fracture. Furthermore, first-principles calculations reveal the fundamental mechanism of domain switching from the atomistic point of view. The main results obtained are summarized as follows.

- (1) Apparent Young's modulus,  $E'$ , and shear modulus of a thin film consisting of  $\text{Ta}_2\text{O}_5$  nanosprings are evaluated as 0.375 and 0.060, respectively. These values are 2-3 orders of magnitude smaller than those of a conventional  $\text{Ta}_2\text{O}_5$  solid thin film. Moreover, the thin film has a strong deformation anisotropy which solid materials cannot attain.
- (2) Vertical stiffness  $k_v$  and lateral stiffness,  $k_l$ , of the single  $\text{Ta}_2\text{O}_5$  nanospring are evaluated as 10.29 and 1.66 N/m, respectively.
- (3) We proposed an experimental technique for evaluating the deformation behavior of a single nanocolumn.
- (4) No stress singularity is found near the free edge of an interface and near the interface crack tip between the thin film consisting of nanosprings and an elastic solid body. The marked stress relaxation is due to the discrete structure of the thin film.



(5) Elimination of the stress singularity owing to the thin film consisting of nanosprings is experimentally demonstrated. The crack initiation at the interface edge is dominated by the apparent stress of the nanospring.

### **References**

- [1] M. Suzuki, Y. Taga, Integrated sculptured thin films, Japanese Journal of Applied Physics, 40 (2001), L358-L359.
- [2] K. Robbie, M.J. Brett and A. Lakhtakia, First Thin-film Realization of A Helicoidal Bianisotropic Medium, J Vacuum Sci Technol A13(6) (1995), 2991-2993.
- [3] H. Hirakata, S. Matsumoto, M. Takemura, M. Suzuki, T. Kitamura, Anisotropic deformation of thin films comprised of helical nanosprings, International Journal of Solids and Structures, 44 (2007), 4030-4038.
- [4] T. Sumigawa, H. Hirakata, M. Takemura, S. Matsumoto, M. Suzuki, T. Kitamura, Disappearance of stress singularity at interface edge due to nanostructured thin film, Engineering Fracture Mechanics, 75 (2008), 3073-3083.
- [5] D.B. Bogy, Edge-bonded Dissimilar Orthogonal Elastic Wedges under Normal and Shear Loading, Journal of Applied Mechanics, 35 (1968), 460.
- [6] T. Sumigawa, T. Sueda, Y. Futamura, M. Suzuki, Takayuki Kitamura, Effect of Interface Layer consisting of Nanosprings on Stress Field near Interface Edge, Engineering Fracture Mechanics, in press.